



Bulletin of the Mineral Research and Exploration

<http://bulletin.mta.gov.tr>



Ilk_inv: a Matlab based algorithm for rapid computation of pseudo-3D density contrast distribution by using Bouguer gravity data

İlkin ÖZSÖZ^{a*}

^aGeneral Directorate of Mineral Research and Exploration, Ankara, Turkey

Research Article

Keywords:

Singular Value Decomposition, Pseudo-3D Density Map, Gravity Modelling.

ABSTRACT

The new generation Matlab-based algorithm provides a rapid estimation of density contrast distribution. The 3D assumption, which is based on the 1D equation, is used. Therefore, the output is called pseudo-3D instead of 3D. The algorithm uses singular value decomposition and the median filter to produce pseudo-3D results. The success of the method is tested by theoretical and field studies. For synthetic studies, single-source models produce reasonable outputs, compared to the true density contrast value. However, the multiple source model shows slight deviations which are $\pm 0.3 \text{ g/cm}^3$, with respect to the true density contrast value. The acceptable results are observed for the Bouguer anomaly of the eastern Mediterranean region. The resolution matrix indicates that the inversion process is biased due to the generalised inverse. The algorithm provides a quite different qualitative interpretation perspective to the interpreter.

Received Date: 05.06.2020

Accepted Date: 23.06.2021

1. Introduction

In geophysics, gravity modeling is can be considered a commonly used method. Tectonic studies (Tontini et al., 2008; Tadjou et al., 2009), resource exploration (Paterson and Reeves, 1985; Allen et al., 2001; Nagihara and Hall, 2001) and engineering solutions (Hinze, 1990; Roberts et al., 1990; Peacock, 1992) can be solved via gravity modelling. Subsurface mass variations generate gravity anomalies. The origin of gravity modeling can be traced back to Newton's Law (Cai et al., 2018). The primary objective of gravity modeling is to detect geometrical and physical parameters of the causative bodies (Grandis and Dahrin, 2014).

Inversion techniques provide the desired parameters by matching the observed data to the theoretical response (Grandis and Dahrin, 2014).

Hence, inversion is a prominent part of the quantitative interpretation of the observed gravity data (Bear et al., 1995; Hinze et al., 2013).

In conventional inversion method, the underground is divided into rectangular prism of unknown density unknown density (Grandis and Dahrin, 2014). Moreover, these prisms should be uniform. Since rectangular blocks are in the same shape and size, estimating densities is a linear inverse problem (Parker, 1977; Grandis and Dahrin, 2014). In other words, there is a linear dependence between data and model parameters (Grandis, 2009; Menke, 2018). This linear relationship can be evaluated as an ill-posed problem.

Errors in the theoretical model and insufficient knowledge about the nature of the potential field cause difficulties during the inversion (Fedi and Rapolla,

Citation Info: Özsoz, İ. 2021. Ilk_inv: a Matlab based algorithm for rapid computation of pseudo-3D density contrast distribution by using Bouguer gravity data. Bulletin of the Mineral Research and Exploration 166, 19-31. <https://doi.org/10.19111/bulletinofmre.959011>

*Corresponding author: İlkin ÖZSÖZ, ilkin.ozsoz@mta.gov.tr

1999). However, the major difficulty for this method is inherent nonuniqueness (Fedi and Rapolla, 1999). Namely, there might be many other models that fit the data (Blakely, 1996; Grandis, 2009). It should be noted that there may be infinite subsurface density distribution models that can generate the observed gravity field (Li and Oldenburg, 1998). Therefore, this technique requires a well-constructed density contrast as an initial model (Li and Oldenburg, 1998). Furthermore, there are many papers that deal with inherent nonuniqueness. Smith (1959, 1960), Parker (1974, 1975) and Hammer et al. (1991) showed that upper and lower bounds of source and density can be uniquely derived by constraining density via analytical equations of known models. There are other papers (Roy, 1962; Parker, 1972; Pedersen, 1977; Pilkington and Crossley, 1986; Xia and Sprowl, 1992; Fedi, 1997) that use nonlinear inversion techniques to estimate the depth and density contrast.

The depth and density contrast of given gravity anomaly can be calculated in either wavenumber domain (Parker, 1972, 1974, 1975; Oldenburg, 1974; Enmark, 1981; Mareschal, 1985; Granser, 1987; Huestis, 1988; Reamer and Ferguson, 1989; Guspi, 1992; Xia and Sprowl, 1992) or spatial domain (Cordell and Henderson, 1968; Al-Chalabi, 1972; Pedersen, 1977, 1979; Tarantola and Valette, 1982; Menichetti and Guillen, 1983). The wavenumber domain methods show effective results deriving the depth between the sedimentary basin and basement rock (Bear et al., 1995). However, determining density distribution cannot be effectively provided with wavenumber domain methods (Bear et al., 1995). On the other hand, the effectiveness of the spatial domain methods is proven in terms of determining subsurface density contrast (Bear et al., 1995).

In this paper, the linear inversion technique in the spatial domain is used with Levenberg-Marquart (Levenberg, 1944) damping factor. The damping parameter prevents the solution from unnecessary outcomes which produce noisy data (Grandis and Dahrin, 2014). Moreover, this parameter provides independence between the initial density contrast model and objective function where geological information is missing (Grandis and Dahrin, 2014).

In general, geophysical problems suffer from ill-posed inverse problems. Stabilization of the inverse problem can be done with singular value

decomposition (SVD) (Press et al., 2007). The SVD method can decompose matrix G into different series of eigen images (Zhao and Chen, 2011). SVD was used for signal and noise separation (Vrabie et al., 2004; Clifford, 2005). Ulrych et al. (1988) and Freire and Ulrych (1988) showed that SVD can be used for separating upgoing and downgoing waves in the vertical seismic profiling (VSP) method.

The inversion method, described in this paper, computes the initial density contrast model from a given gravity field. Then, it applies a linear inversion technique using SVD to estimate the final density contrast model.

2. Methods

The fundamental theory of linear density inversion algorithm is based on Bott (1960) and Cordell and Henderson (1968). Nevertheless, it should be noted that the algorithm has undergone slight adjustments. The workflow of the algorithm is displayed in Figure 1.

$$\Delta\rho = \frac{g_j}{2\pi G t_j} \quad (1)$$

where g_j is the gravity field of the infinite slab whose thickness is t_j and density contrast is $\Delta\rho$ and G is the universal gravitational constant.

Basically the algorithm can be divided into three fundamental steps:

The first step of the method is computing the initial density contrast map from a given thickness value using Equation (1). Furthermore, an optional background density contrast value might be selected. This parameter allows the interpreter to mask the contribution of the density values above the slab.

The second step involves SVD inversion fit and moving median filtering. The output of the inversion provides slight changes in the initial density contrast map. Furthermore, the median filter removes sharp variations from the output. The final density contrast map is obtained.

The last phase of the estimation is assessing the quality of inversion by resolution and covariance matrices.

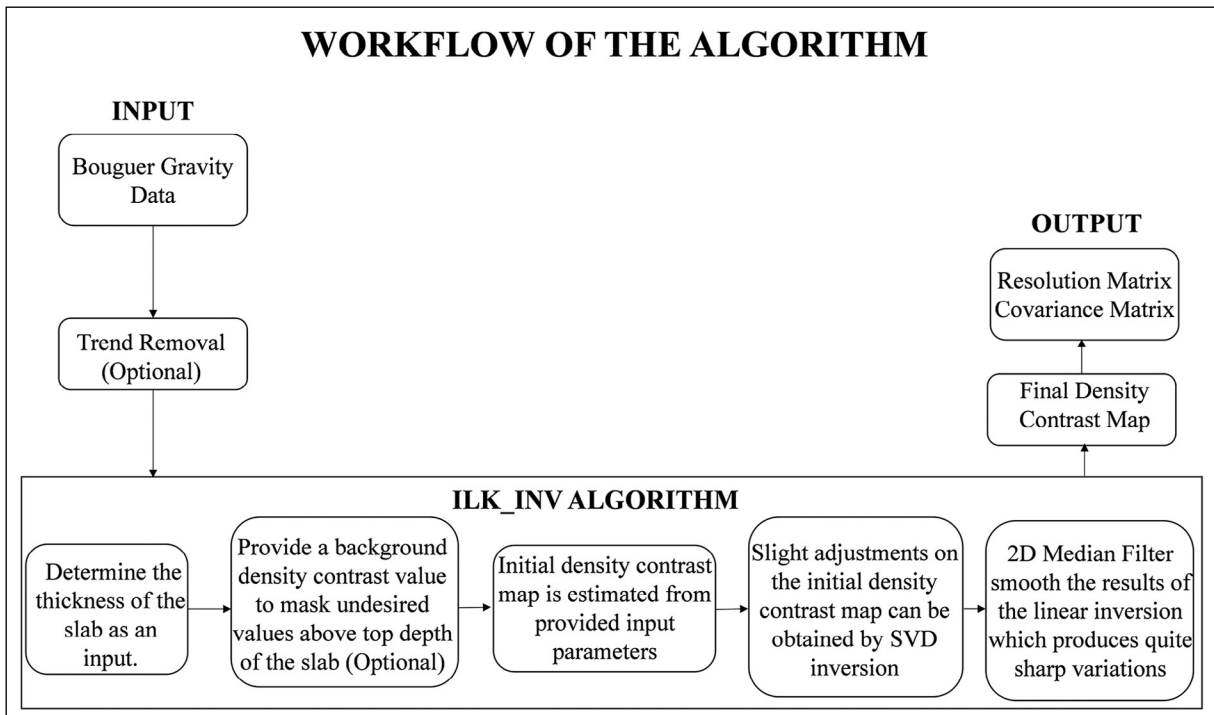


Figure 1- Workflow of the ilk_inv algorithm.

2.1. Singular Value Decomposition (SVD)

Observations, d , can be calculated by a simple forward modeling equation which can be constructed by using Kernel matrix, G , and geometrical or physical parameters of the source, m . This equation can be written as:

$$d = G * m \tag{2}$$

The initial model is calculated from the given thickness and calculated constant density contrast from 1D Bouguer Slab formula and observed gravity. Equation 1 can be used for calculating the gravity anomaly over a constant thickness and variable density. The difference between theoretical values, calculated from Equation 2, and observed values can be written as Δg_B . Hence (2) can be modified as:

$$\Delta g_B = G \Delta \rho \tag{3}$$

where $\Delta \rho$, difference between initial and estimated density distribution. For n number of observations and m number of parameters, the length of Δg_B and $\Delta \rho$ is $(n * 1)$ $(n * m)$ and $(m * 1)$, respectively.

According to Lawson and Hanson (1974), matrix G can be decomposed into data space, model space

and singular values via SVD. Furthermore, the SVD can be used for solving ill-conditioned and/or rank deficient inverse problems (Strang, 1988; Golub and Van Loan, 1996; Lanczos, 1997). The matrix G can be factored into;

$$G = USV^T \tag{4}$$

where U is an $(n * n)$ orthogonal matrix whose vectors are spanning the data space, V is an $(m * m)$ orthogonal matrix whose vectors are spanning the model space and S is $(m * n)$ diagonal matrix of the singular values (Aster et al., 2018). It should be noted that some singular values might be zero. If nonzero singular values are called S_q , S can be partitioned as;

$$S = \begin{bmatrix} S_q & 0 \\ 0 & 0 \end{bmatrix} \tag{5}$$

where S_q is $(q * q)$ matrix that has positive singular values. Hence, matrix G can be modified as;

$$G = [U_q \ U_0] \begin{bmatrix} S_q & 0 \\ 0 & 0 \end{bmatrix} [V_q \ V_0]^T \tag{6}$$

$$G = U_q S_q V_q^T \tag{7}$$

where the size of U_q and V_q are $(n * q)$ and $(m * q)$. According to Aster et al. (2018), U_0 and V_0 contribute

nothing to matrix G. Furthermore, if V_0 is multiplied by any model, observations are not affected. The result will appear in the model null space. On the other hand, if $d_{obs} = d + \alpha U_0$, d_{obs} cannot be exactly fit by any model. In other words, there is a data component in the data null space. Table 1 shows the effect of data null space and model null space on the uniqueness and data fit (Menke, 1984).

In this paper, case number 4 is used. Since the exact fit cannot be provided, the damping factor should be used to avoid overfitting (Grandis and Dahrin, 2014). The over-fitting problem results from the residual model solutions. Damping parameter can be determined by a trial-error approach or eigenvalues of GG^T . Density distribution can be estimated from the following equation:

$$S_{qq} = \frac{(\lambda^2 + S_q^2)}{\lambda} \quad (8)$$

$$\Delta\rho_e = V_q S_{qq}^{-1} U_q^T \Delta g_B \quad (9)$$

where λ is the damping parameter and $\Delta\rho_e$ is the estimated density contrast.

2.2. Resolution and Covariance Matrix

The generated model can be tested in terms of how the model represents the true situation (Aster et al., 2018). It is known that the least square estimator is unbiased. However, the generalised inverse solution cannot be considered as an unbiased estimator (Aster et al., 2018). The bias can be measured by a model resolution matrix (Aster et al., 2018). The calculation of covariance and model resolution matrices is shown in the following equations;

$$C = G^\Phi cov(\Delta g_B) (G^\Phi)^T \quad (10)$$

$$R = V_q V_q^T \quad (11)$$

where C is a covariance matrix and R is the resolution matrix. Basically, the resolution matrix can associate the biased true solution with the estimated parameters. It is prominent that the resolution matrix cannot be related to the data and data errors (Vasco, 1989). It is the function of the geometry of the survey or properties of G (Vasco, 1989; Aster et al., 2018). If matrix G is not rank deficient and zero, the resolution matrix will be an identity matrix (Vasco, 1989). In this paper, zero values of U_q , V_q and S_q are not taken into account. Therefore, the resolution matrix is not an identical matrix. However, it is worth noting that this is an unbiased solution. Moreover, the covariance matrix provides a map of Gaussian errors (Vasco, 1989).

2.3. Median Filter

Linear filtering can be used for suppressing the noise in the signal. The simple linear filter uses the mean value of the selected dataset along a sliding window (Arias - Castro and Donoho, 2009). However, this type of filter has a major drawback at the edges of the structures (Church et al., 2008).

Furthermore, smooth low-pass filtering is useful for eliminating sharp points and noise. Nevertheless, this type of filter may produce blurring on a geophysical image in some cases.

Hence, Tukey (1974) introduced an alternative concept of linear filtering. As it is known that median is the centre value of the given series. In certain situations, median filtering has two major advantages. Firstly, it can preserve information on structures with a sharp edge (Justusson, 1981). Secondly, outliers and spikes can be reasonably suppressed with a median filter (Justusson, 1981, Arias-Castro and Donoho, 2009).

Table 1- Generalised inverse solution for different cases where G^Φ indicates the generalised inverse.

Case Number	Case	Uniqueness	Data Fit	Solution
1	$U = U_q$ $V = V_q$	UNIQUE	EXACT FIT	$G^\Phi = (U_q S_q V_q^T)^{-1}$
2	$U = U_q$ V_q is not square	NON-UNIQUE	EXACT FIT	$G^\Phi = G^T (GG^T)^{-1}$ Minimum Norm Solution
3	$V = V_q$ U_q is not square	UNIQUE	NOT EXACT FIT	$G^\Phi = (G^T G)^{-1} G^T$ Least-Squares Solution
4	U_q is not square V_q is not square	NON-UNIQUE	NOT EXACT FIT	Use generalised inverse. $G^\Phi = V_q S_q^{-1} U_q^T$

If the length of the median filter is even, the average of the multiple centre values can be used. On the other hand, it is recommended to use the median filter whose length is odd (Church et al., 2008). The median filter can be performed by taking the median of the windowed series. Then, the median value is used to replace the studied point. Figure 2 illustrates a schematic application of N-length and N * N sized median filter.

The effect of the median filter is tested on the random dataset. Different lengths of 1D median filters are applied to the dataset. Figure 3 demonstrates the results of the median filter, whose length is 3, 5 and 7, on the random data.

As it is shown in Figure 3, median filtering suppresses outliers and extreme points. It reveals the true extremum points of the noisy data. Spiky points are removed but smoother extreme points are preserved. In this paper, the median filter is required for masking the outliers and spiky points. The major drawback of the algorithm on the gridded data is outliers and spiky points. These extreme points are filtered out by using 2D median filtering.

3. Synthetic Studies

In order to analyse the effectiveness of the proposed method, three different synthetic models and

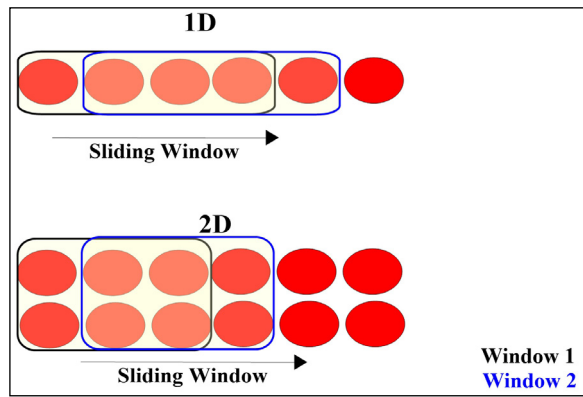


Figure 2- Application of 1D (N=3) and 2D (N=3*3) median filtering.

field data are used. Synthetic models include a single prism with positive density contrast, multiple prisms with positive density contrast and a 3D cylinder model with negative density contrast. The produced synthetic studies are not contaminated by Gaussian error. Field data set is obtained from the International Gravimetric Bureau.

3.1. Single Prism with Positive Density Contrast

The gravity anomaly of a single prism is calculated within $100 * 100 \text{ km}^2$ area. The top and bottom depths of the prism are 3 and 5 km, respectively. Prism has a $+1 \text{ g/cm}^3$ density contrast with respect to the

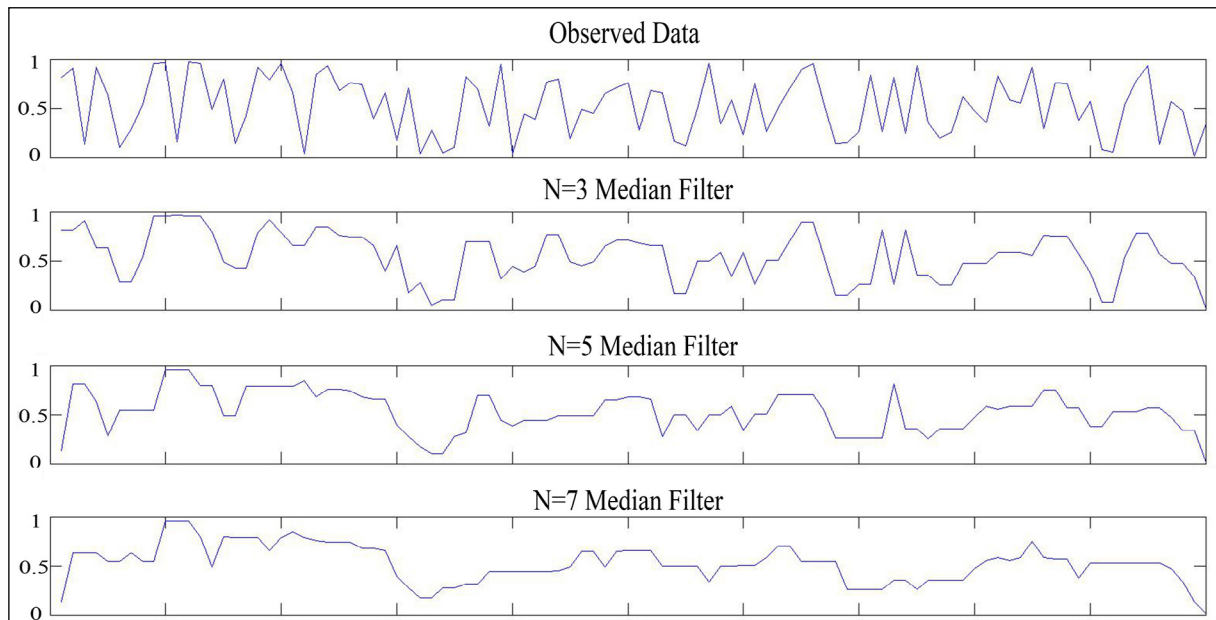


Figure 3- Effect of the median filter and its length on the fluctuating random dataset.

background density. Matlab-based program (ilk_inv) is used for producing density contrast of the prism.

The gravity field of prism and gridding interval along x and y axes assumed background density contrast (optional) and thickness are used as an input parameter. The description of the model is demonstrated in Figure 4.

Regarding the input parameters, 1 km grid spacing in both x and y directions is used for 100 * 100 km² area. A slab thickness value is required for the calculation. In this case, thickness is chosen as 3 km, which increases the accuracy of the output.

The Matlab-based algorithm (ilk_inv) can produce two major outputs which are the initial density contrast and final density contrast. The output of the ilk_inv for the gravity anomaly of a single prism with positive density contrast is shown in Figure 5.

3.2. Multiple Prisms with Positive Density Contrast

In this synthetic example, two different prisms which have different top and bottom depths are used within 100 * 100 km² area. The top and bottom depths of prism 1 are 2 km and 6 km respectively. Prism 1 has a +0.3 g/cm³ density concerning the background density. Additionally, the top and bottom depths of Prism 2 are 7 km and 11 km correspondingly. Prism 2 has a +0.8 g/cm³ density contrast for the background density. The geometrical and physical parameters of the model are shown in Figure 6.

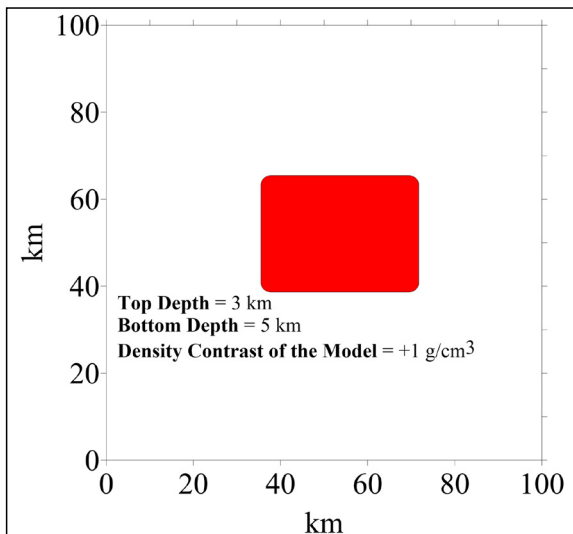


Figure 4- Physical and geometrical parameters of the single prism synthetic model.

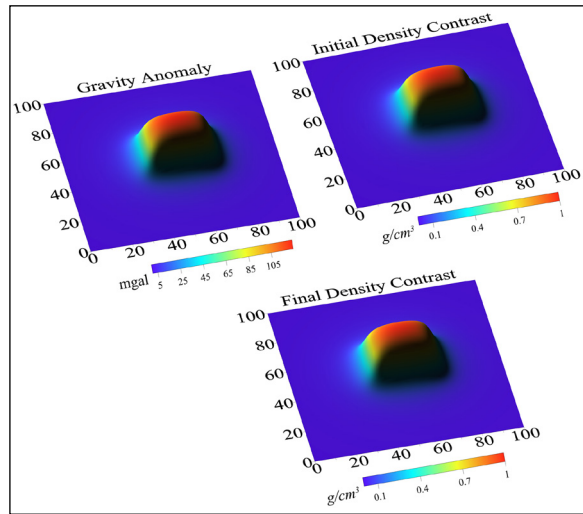


Figure 5- Products of ilk_inv for a single prism with positive density contrast.

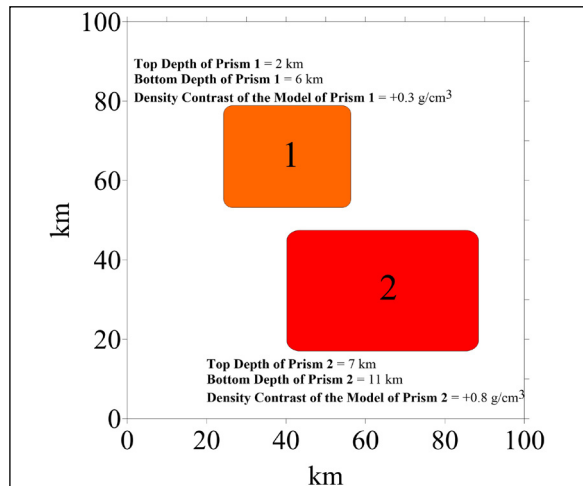


Figure 6- Physical and geometrical parameters of the multiple prism synthetic model.

The slab thickness is chosen 7 km (top depth of the deeper prism) since the deeper source controls the density distribution for this synthetic model. The outputs for the selected input parameters are shown in Figure 7.

3.3. 3D Cylinder Model with Negative Density Contrast

A synthetic cylinder model which is surrounded by sedimentary rocks is used within 100 * 100 km² area. The top and bottom depths of the cylinder model are 10 and 12 km. The density contrast of the cylinder is -0.3 g/cm³. The parameters of this synthetic model are indicated in Figure 8.

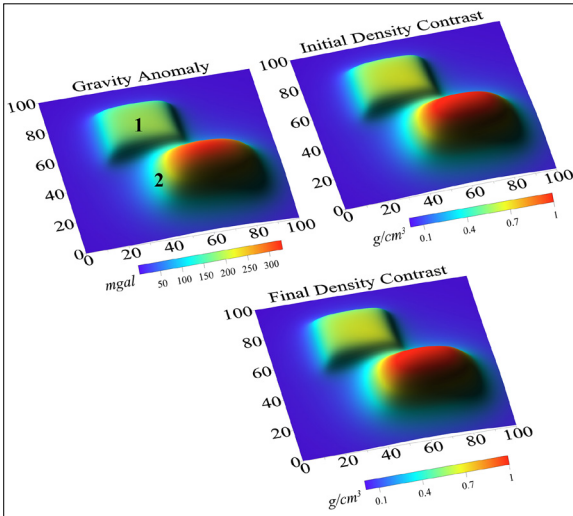


Figure 7- Outputs of ilk_inv for multiple prisms with positive density contrast.

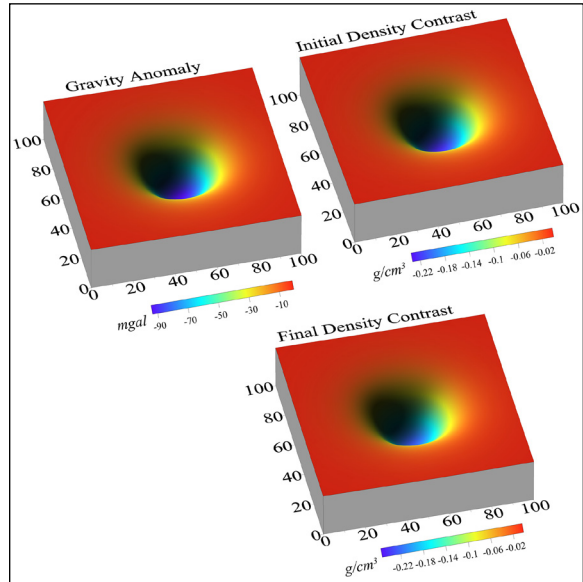


Figure 9- Products of the synthetic cylinder model with negative density contrast.

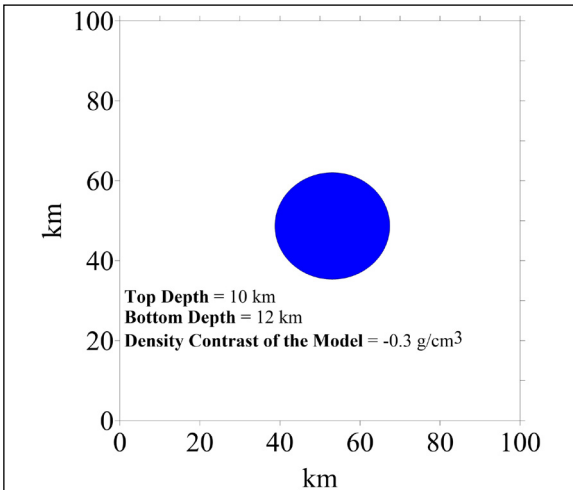


Figure 8- Physical and geometrical parameters of the cylinder synthetic model.

The slab thickness is chosen 10 km since it corresponds to the top depth of the cylinder model. The output of ilk_inv for the cylinder model covered by sedimentary rocks is demonstrated in Figure 9.

4. Field Study

4.1. Tectonic Setting of the Study Area

Eastern Mediterranean tectonics resulted from tectonic movements of African, Eurasian and Arabian plates. The W - SW movement of the Anatolian Block can be associated with extension in Western Anatolia, compression in Eastern Anatolia and

faulting throughout the North and East Anatolian fault zones, and movement of the African Plate relative to the Eurasian Plate formed Hellenic Subduction Zone (McKenzie, 1972; Le Pichon and Angelier, 1979; McClusky et al., 2000; Mart and Ryan, 2003; Pamukçu, 2016; Kahveci et al., 2019). A major subduction along the Hellenic Arc stems from the roll-back mechanism under the Aegean Sea (Le Pichon and Angelier, 1979; Le Pichon, 1983; Sorel et al., 1988; Mercier et al., 1989; Kahveci et al., 2019).

The Hellenic Arc comprises three trenches, Helen, Pliny and Strabo. These trenches formed 3500 - 4000 m depth in the Mediterranean Sea. Fairly variable bathymetric values are observed in the southern part of the Hellenic Arc (Gönenç and Akgün, 2012). Furthermore, the southern part of Crete is characterised by active seismicity at 20 - 40 km depth (Delibasis et al., 1999; Meier et al., 2004). Additionally, studies of Papazachos et al. (2000) and Gönenç et al. (2006) showed that Wadati - Benioff Zone reaches 150 - 200 km depth owing to the northward movement of the Hellenic Arc.

4.2. Geophysical Findings

The eastern Mediterranean region is studied. The field gravity data is obtained from the International Gravimetric Bureau (BGI). The gravity data is part of the World Gravity Map (WGM 2012) (Bonvalot et al., 2012).

Briefly, WGM 2012 data is derived from the EGM2008 geopotential model and ETOPO1 model (Bonvalot et al., 2012). WGM 2012 handles regional and global variations in the gravity field of the Earth. WGM 2012 provides free-air, Bouguer and isostatic anomalies. In this study, the Bouguer anomaly is required. The Bouguer anomaly of the study was given in Figure 10.

If the slab thickness is chosen too shallow regarding the resolution of data, the output will be an exaggerated density contrast map. Since the resolution of WGM 2012 is not as high as land gravity data, the slab thickness is tried to be chosen from the long-wavelength component of the data. The outputs were demonstrated in Figure 11.

In order to examine the success of the inversion process and the effect of the Gaussian errors on the solution, resolution and covariance matrices should

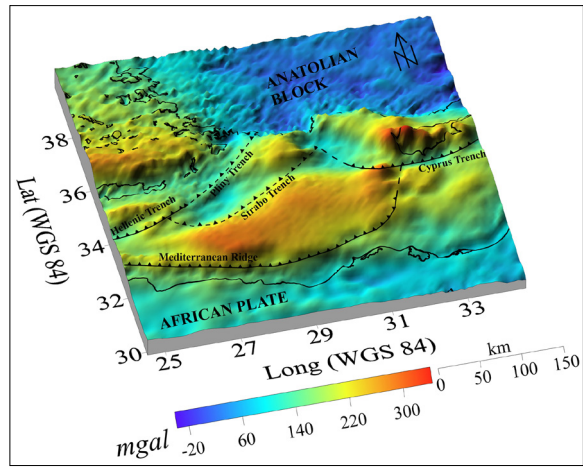


Figure 10- Bouguer anomaly of the East Mediterranean region with the major tectonic elements (Lat: latitude, Long: longitude; Dilek, 2006; Öner et al., 2010).

be analysed. Figure 12 illustrates the covariance and resolution matrices for the field data.

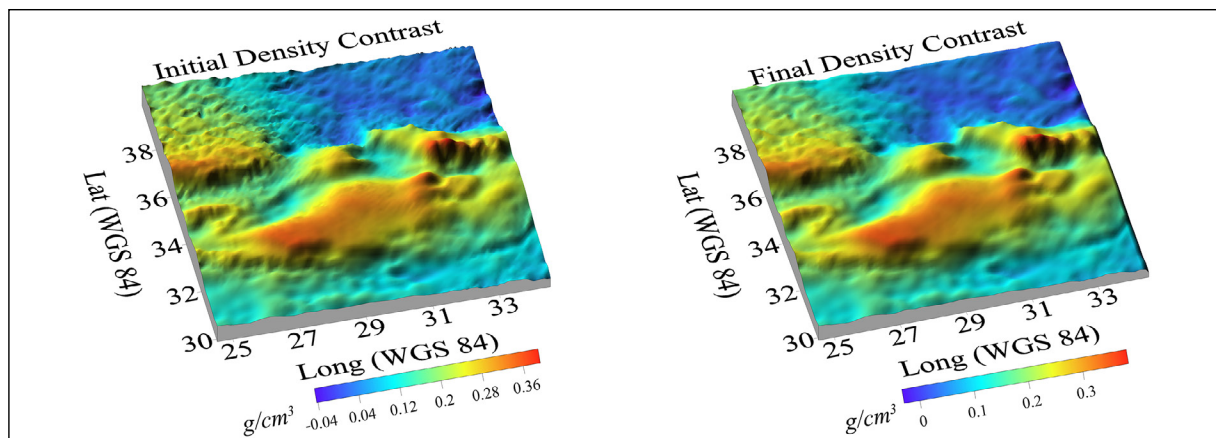


Figure 11- Estimated density contrast maps map for the eastern Mediterranean region (Lat: latitude, Long: longitude).

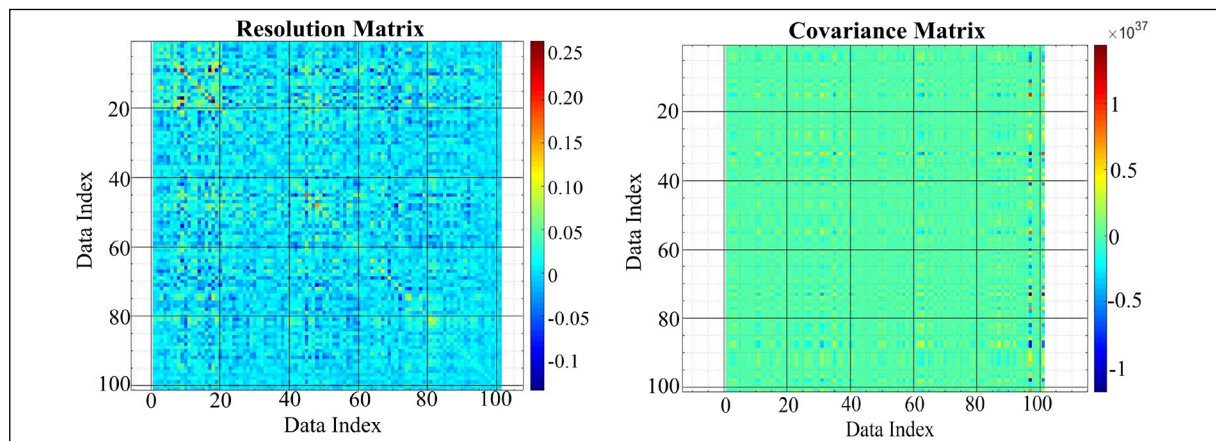


Figure 12- Resolution and covariance matrices.

Furthermore, the validity of this approach can be illustrated by calculating RMS error between estimated gravity data and observed data. Figure 13 indicates how computed gravity data from pseudo-3D density contrast match the observed gravity data. As it can be seen from Figure 13, the calculated RMS error is 8.63 mgal.

Since gravity data and density values are linearly correlated, interrelationship between the gravity inversion results and the satellite gravity data is considerably high. It can be said that the gravity inversion results are a smoothed representation of the observed gravity data. Strabo Trench, Hellenic Trench, Pliny Trench, Cyprus Trench and Mediterranean Ridge are adequately represented in the inversion results as well as the gravity data.

Geologically, the subducting plate is characterised by higher density contrast in the gravity inversion results. To exemplify, the southern part of the Strabo Trench which is a subducting plate is represented by higher density contrast and gravity anomaly.

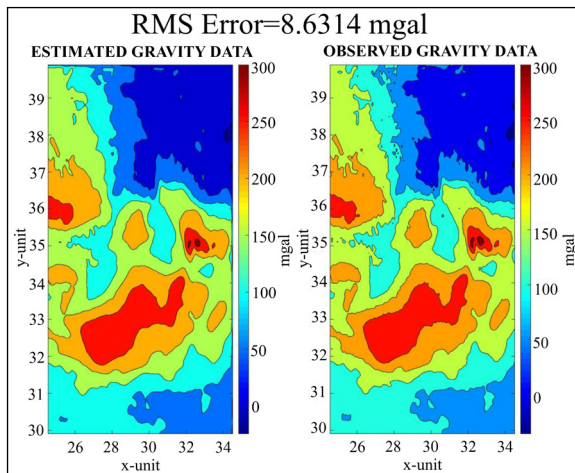


Figure 13- Comparison of estimated and observed gravity anomaly.

5. Discussion

The density contrast map is computed by the `ilk_inv` algorithm. The algorithm uses 1D Bouguer Slab Formula to produce a constant initial density value and SVD for modelling the gravity field and estimating the density contrast. Then it applies a 2D median filter to the estimated values in order to remove sharp variations. It is worth noting that the algorithm cannot produce 3D estimations. It only imitates 3D estimations.

The input parameters are the slab thickness, grid spacing and background density contrast (optional). The slab thickness value must be a positive number. Grid spacing parameter along x and y direction has a major impact on the computation time. It is recommended to use optimum grid spacing since extremely small grid spacing does not improve results. The optional background density contrast can be chosen with a specific value or 0 g/cm^3 . If it is chosen as 0 g/cm^3 , the result shows the raw computed density contrast map with respect to 0 g/cm^3 . On the other hand, if a background density contrast is used, the background density effect on the geological structures can be filtered. It is recommended to use background density contrast value in case that lithological information of the study area is well-known.

Various synthetic models and a field model is used for testing the success of the `ilk_inv` algorithm. The first synthetic study, a single prism with positive density contrast, produced fairly reliable results. The initial density contrast and final density contrast value are almost the same since the data are not contaminated by noise. The final density contrast map found the density contrast of prism 1 g/cm^3 , corresponding to the true density contrast value. For obtaining the best result, slab thickness should be similar to the top depth of the basement rock.

The second synthetic study, multiple prisms with positive density contrast, produced slightly acceptable results. Similar to the first synthetic study, initial and final density contrasts cannot be distinguished. Prism 2 is located deeper than Prism 1. Furthermore, the density contrast of Prism 1 is dominant. Therefore, the depth of the Prism 2, 7 km, ought to be used as slab thickness. Prism 2 can be considered as a basement rock. It can be said that if there are two dominant sources in the study area, the produced results might contain moderate uncertainty.

The final synthetic study evaluates the reliability of the algorithm in terms of modelling structures with negative density contrast. The final density contrast of the cylinder model is roughly -0.23 g/cm^3 and it deviates from the true density contrast, -0.3 g/cm^3 . It might be said that the algorithm tends to produce slightly deviated results from the true density contrast while computing a model with a negative density contrast.

The other prominent observation is the difference between initial and final density contrast maps. It is clear that the final density contrast map converges true density contrast value with slight uncertainty.

Apart from the synthetic study, the field data is used for the evaluation of the algorithm. Eastern Mediterranean gravity data is used as a field data example. There is a considerable positive anomaly, 300 mgal, at the south-western part of the Cyprus region. It can be said that a positive density contrast anomaly will be observed around the same region because of a positive correlation between estimated density contrast and the observed gravity anomaly.

The slab thickness for the field study is chosen as 20 km. Since the gravity data have limited resolution and are dominated by considerably long wavelengths, crustal scale inversion over the large study area would be more suitable. If density contrast maps, initial and final density contrast, at 20 km are compared, it can be said that the final density contrast map is substantially smoother than the initial density contrast map. Namely, if the thickness is chosen significantly deep, variations in the long wavelength component are dominant rather than short wavelength components in the computed density contrast map.

The validity of the approach is tested by comparison of estimated and observed gravity anomalies. If Figure 13 is analysed, the estimated gravity data produces smoother results than observed gravity data as the estimated gravity anomaly is computed from median filtered pseudo-3D density contrast values. It can be said that the anomalies related to the small wavelength components cannot be modelled in an estimated gravity anomaly map. However, longer wavelength components are modelled successfully.

The amount of bias and distribution of errors can be evaluated via resolution and covariance matrices. Since it is a biased solution, the resolution of the solution is quite low. The bias in the solution is related to the generalised inverse operator. Nonetheless, this operator is required for solving the inverse problem. For the unbiased solution, the identity matrix is required as a resolution matrix. In this case, the output of the algorithm is the biased pseudo-3D distribution of density contrast. Consequently, since the algorithm is biased and the solution is not actually 3D, the resolution of the solution produces significantly low

values. Additionally, the covariance matrix presents quite high values in some parts of the solution. It is clear that the Gaussian errors increase certain data indexes.

The regional tectonic structures in the field study, Hellenic Trench, Pliny Trench, Strabo Trench, Mediterranean Ridge and Cyprus Trench, are clearly represented on the Bouguer Gravity Anomaly (Figure 10a).

Initial and final density contrast maps have a linear relationship with the observed gravity anomaly. However, these maps can indicate density contrast between sediment accumulation zones and basement rocks, which is roughly $0.2 - 0.4 \text{ g/cm}^3$.

The output is considerably dependent on the input data rather than the damped inversion process. If input data is dominated by the longer wavelengths, the result will be smooth. On the other hand, if data have relatively short wavelengths, the produced output will be relatively sharp.

The algorithm is directly associated with the residual gravity anomaly and indirectly related with the actual density variations. Therefore, it cannot produce entirely reliable density variations for the complex tectonics even if you have noise-free data. It is designed for obtaining regional density contrast for the large study area. The regional density contrast, obtained from the algorithm, can be used as initial density contrast values or constraining parameters. Also, if the output is used as a constraining parameter, it is highly possible to reduce the effect of non-uniqueness.

6. Results

Rapid pseudo-3D computation of density contrast map can be done by the `ilk_inv` algorithm. Theoretical studies showed that if there is a single dominant source in the survey area, estimations are reliable. However, the estimation of density contrast slightly diverges from the true density contrast if there are multiple dominant sources.

The computed density contrast map from the field study reflects the same spectral characteristics of the observed gravity data and crustal thickness. The density contrast map indicated that density variation

between sediment accumulation zones and basement rocks is approximately $0.2 - 0.4 \text{ g/cm}^3$.

The algorithm presents a fast computation of density contrast automated initial estimation. It computes the initial estimation from the given Bouguer Anomaly. However, the final and initial estimation outputs are quite similar in some cases. Furthermore, it requires few parameters to compute density contrast distribution. Nevertheless, the major limitation is that the algorithm assumes the output is 3D by using a calculated initial density from the 1D equation. The outputs contain all limitations of the 1D formula. Since the algorithm uses generalised inverse the outputs are biased. Therefore, the resolution matrix produces poor results. The other limitation is the inversion process is linear which means estimated density contrast map and observed data has a linear relation. Even though the outputs are reasonable, the limitations of the method should be taken into account for the interpretation step.

Acknowledgements

I would like to offer my special thanks to Dr. Chris GREEN for his insightful contributions to the theory of the algorithm. Moreover, I am grateful to anonymous reviewers for their comments.

References

- Al Chalabi, M. A. 1972. Interpretation of gravity anomalies by non-linear optimisation. *Geophysical Prospecting* 20(1), 1-16.
- Allen, T. I., Cooper, S. A., Cull, J. P. 2001. High definition gravity surveys and density modelling for kimberlite exploration. *Exploration Geophysics* 32(2), 89-94.
- Arias Castro, E., Donoho, D. L. 2009. Does median filtering truly preserve edges better than linear filtering?. *The Annals of Statistics* 37(3), 1172-1206.
- Aster, R. C., Borchers, B., Thurber, C. H. 2018. *Parameter Estimation and Inverse Problems*. Elsevier.
- Bear, G. W., Al-Shukri, H. J., Rudman, A. J. 1995. Linear inversion of gravity data for 3-D density distributions. *Geophysics* 60(5), 1354-1364.
- Blakely, R. J. 1996. *Potential Theory in Gravity and Magnetic Applications*. Cambridge University Press.
- Bonvalot, S., Balmino, G., Briais, A., Kuhn, M., Peyrefitte, A., Vales, N., Biancale, R., Gabalda, G., Reinquin, F. 2012. World Gravity Map: a set of global complete spherical Bouguer and isostatic anomaly maps and grids. *International European Geosciences Union General Assembly Conference Abstracts* 14, 11091.
- Bott, M. H. P. 1960. The use of rapid digital computing methods for direct gravity interpretation of sedimentary basins. *Geophysical Journal International* 3(1), 63-67.
- Cai, Y.F., Li, C., Saridakis, E. N., Xue, L. Q. 2018. f(T) gravity after GW170817 and GRB170817A. *Physical Review* 97(10), 103513.
- Church, J. C., Chen, Y., Rice, S. V. 2008. A spatial median filter for noise removal in digital images. *Institute of Electrical and Electronics Engineers Southeast Conference*, 618-623.
- Clifford, G. D. 2005. Singular value decomposition and independent component analysis for blind source separation. *Biomedical, Signal Image Process* 44, 489-499.
- Cordell, L., Henderson, R. G. 1968. Iterative three-dimensional solution of gravity anomaly data using a digital computer. *Geophysics* 33(4), 596-601.
- Delibasis, N., Ziazia, M., Voulgaris, N., Papadopoulos, T., Stavrakakis, G., Papanastassiou, D., Drakatos, G. 1999. Microseismic activity and seismotectonics of Heraklion area (central Crete Island, Greece). *Tectonophysics* 308(1-2), 237-248.
- Dilek, Y. 2006. Collision tectonics of the Mediterranean region: causes and consequences. *Geological Society of America Special Papers* 409, 1.
- Enmark, T. 1981. A versatile interactive computer program for computation and automatic optimization of gravity models. *Geoexploration* 19(1), 47-66.
- Fedi, M. 1997. Estimation of density, magnetization, and depth to source: a nonlinear and noniterative 3-D potential-field method. *Geophysics* 62(3), 814-830.
- Fedi, M., Rapolla, A. 1999. 3-D inversion of gravity and magnetic data with depth resolution. *Geophysics* 64(2), 452-460.
- Freire, S. L., Ulrych, T. J. 1988. Application of singular value decomposition to vertical seismic profiling. *Geophysics* 53(6), 778-785.
- Golub, G. H., Van Loan, C. F. 1996. *Matrix Computations*. Johns Hopkins University Press, Baltimore, London.

- Gönenç, T., Akgün, M., Ergün, M. 2006. Girit yayının sismolojik ve bouguer gravite anomalisi verilerine göre yorumlanması. *Geosound* 48(1), 51-68.
- Gönenç, T., Akgün, M. 2012. Structure of the Hellenic subduction zone from gravity gradient functions and seismology. *Pure and Applied Geophysics* 169(7), 1231-1255.
- Grandis, H. 2009. Introduction to Geophysical Inversion Modeling. Indonesia Geophysical Expert Association (HAGI).
- Grandis, H., Dahrin, D. 2014. Constrained two-dimensional inversion of gravity data. *Journal of Mathematical and Fundamental Sciences* 46(1), 1-13.
- Granser, H. 1987. Nonlinear inversion of gravity data using the Schmidt-Lichtenstein approach. *Geophysics* 52(1), 88-93.
- Guspi, F. 1992. Three-dimensional Fourier gravity inversion with arbitrary density contrast. *Geophysics* 57(1), 131-135.
- Hammer, P. T. C., Hildebrand, J. A., Parker, R. L. 1991. Gravity inversion using semi-norm minimization: density modeling of Jasper Seamount. *Geophysics* 56(1), 68-79.
- Hinze, W. J. 1990. Geotechnical an Environmental Geophysics. SEG, I, 75-126.
- Hinze, W. J., Von Frese, R. R., Saad, A. H. 2013. Gravity and Magnetic Exploration: Principles, Practices, and Applications. Cambridge University Press.
- Huestis, S. P. 1988. Uniform norm minimization for two-signed solutions. *Geophysics* 53(5), 721-722.
- Justusson, B. I. 1981. Median Filtering: Statistical Properties. In *Two-Dimensional Digital Signal Processing II*. Springer, Heidelberg, Berlin, 161-196.
- Kahveci, M., Çırmık, A., Doğru, F., Pamukçu, O., Gönenç, T. 2019. Subdividing the tectonic elements of Aegean and Eastern Mediterranean with gravity and GPS data. *Acta Geophysica* 67(2), 491-500.
- Lanczos, C. 1997. Linear Differential Operators. Society for Industrial and Applied Mathematics, 564.
- Lawson, C. L., Hanson, R. J. 1974. Solving Least Squares Problems. Society for Industrial and Applied Mathematics, U.S., 350.
- Le Pichon, X. 1983. Land-locked oceanic basins and continental collision: the eastern Mediterranean as a case example. Hsu, K. (Ed.) *Mountain Building*, Academic Press, London, 201-211.
- Le Pichon, X., Angelier, J. 1979. The Hellenic arc and trench system: a key to the neotectonic evolution of the eastern Mediterranean area. *Tectonophysics* 60(1-2), 1-42.
- Levenberg, K. 1944. A method for the solution of certain nonlinear problems. *Quarterly Applied Mathematics* 2, 164-168.
- Li, Y., Oldenburg, D. W. 1998. 3-D inversion of gravity data. *Geophysics* 63(1), 109-119.
- Mareschal, J. C. 1985. Inversion of potential field data in Fourier transform domain. *Geophysics* 50(4), 685-691.
- Mart, Y., Ryan, W. 2003. The tectonics of Cyprus Arc: a model of complex continental collision. *European Geophysical Society - American Geophysical Union - European Union of Geosciences Joint Assembly*, 2282.
- McClusky, S., Balassanian, S., Barka, A., Demir, C., Ergintav, S., Georgiev, I., Gürkan, O., Hamburger, M., Hurst, K., Kahle, H., Kastens, K. 2000. Global positioning system constraints on plate kinematics and dynamics in the eastern Mediterranean and Caucasus. *Journal of Geophysical Research: Solid Earth* 105(B3), 5695-5719.
- McKenzie, D. 1972. Active tectonics of the Mediterranean region. *Geophysical Journal International* 30(2), 109-185.
- Meier, T., Rische, M., Endrun, B., Vafidis, A., Harjes, H. P. 2004. Seismicity of the Hellenic subduction zone in the area of western and central Crete observed by temporary local seismic networks. *Tectonophysics* 383(3-4), 149-169.
- Menichetti, V., Guillen, A. 1983. Simultaneous interactive magnetic and gravity inversion. *Geophysical Prospecting* 31(6), 929-944.
- Menke, W. 1984. *Geophysical Data Analysis. Discrete Inverse Theory*. Academic Press, New York, 312.
- Menke, W. 2018. *Geophysical Data Analysis: Discrete Inverse Theory*. Academic Press, New York.
- Mercier, J. L., Sorel, D., Vergely, P., Simeakis, K. 1989. Extensional tectonic regimes in the Aegean basins during the Cenozoic. *Basin Research* 2(1), 49-71.
- Nagihara, S., Hall, S. A. 2001. Three-dimensional gravity inversion using simulated annealing: constraints on the diapiric roots of allochthonous salt structures. *Geophysics* 66(5), 1438-1449.
- Oldenburg, D. W. 1974. The inversion and interpretation of gravity anomalies. *Geophysics* 39(4), 526-536.
- Öner, Z., Dilek, Y., Kadioğlu, Y. K. 2010. Geology and geochemistry of the synextensional salihli granitoid in the Menderes core complex, western Anatolia, Turkey. *International Geology Review* 52(2-3), 336-368.

- Pamukçu, O. 2016. Geodynamic assessment of eastern Mediterranean region: a joint gravity and seismic b value approach. *Arabian Journal of Geosciences* 9(5), 360.
- Papazachos, B. C., Karakostas, V. G., Papazachos, C. B., Scordilis, E. M. 2000. The geometry of the Wadati–Benioff zone and lithospheric kinematics in the Hellenic arc. *Tectonophysics* 319(4), 275-300.
- Parker, R. L. 1972. The rapid calculation of potential anomalies. *Royal Astronomical Society Geophysical Journal*, 31.
- Parker, R. L. 1974. Best bounds on density and depth from gravity data. *Geophysics* 39(5), 644-649.
- Parker, R. L. 1975. The theory of ideal bodies for gravity interpretation. *Geophysical Journal International* 42(2), 315-334.
- Parker, R. L. 1977. Understanding inverse theory. *Annual Review of Earth and Planetary Sciences* 5(1), 35-64.
- Paterson, N. R., Reeves, C. V. 1985. Applications of gravity and magnetic surveys: The state-of-the-art in 1985. *Geophysics* 50(12), 2558-2594.
- Peacock, R. J. 1992. Cavity detection? an engineering application for gravity. *Exploration Geophysics* 23(4), 567-570.
- Pedersen, L. B. 1977. Interpretation of potential field data a generalized inverse approach. *Geophysical Prospecting* 25(2), 199-230.
- Pedersen, L. B. 1979. Constrained inversion of potential field data. *Geophysical Prospecting* 27(4), 726-748.
- Pilkington, M., Crossley, D. J. 1986. Determination of crustal interface topography from potential fields. *Geophysics* 51(6), 1277-1284.
- Press, W. H., Teukolsky, S. A., Vetterling, W. T., Flannery, B. P. 2007. *Numerical Recipes 3rd Edition: The Art of Scientific Computing*. Cambridge University Press.
- Reamer, S. K., Ferguson, J. F. 1989. Regularized two-dimensional Fourier gravity inversion method with application to the Silent Canyon caldera, Nevada. *Geophysics* 54(4), 486-496.
- Roberts, R. L., Hinze, W. J., Leap, D. I., Ward, S. H. 1990. Application of the gravity method to the investigation of a landfill in glaciated midcontinent, USA. *Geotechnical and Environmental Geophysics* 2, 253-260.
- Roy, A. 1962. Ambiguity in geophysical interpretation. *Geophysics* 27(1), 90-99.
- Smith, R. A. 1959. Some depth formulae for local magnetic and gravity anomalies. *Geophysical Prospecting* 7(1), 55-63.
- Smith, R. A. 1960. Some formulae for interpreting local gravity anomalies. *Geophysical Prospecting* 8(4), 607-613.
- Sorel, D., Mercier, J. L., Keraudren, B., Cushing, M. 1988. Le rôle de la traction de la lithosphère subductée dans l'évolution géodynamique plio-pléistocène de l'arc égéen: mouvements verticaux alternés et variations du régime tectonique. *Comptes rendus de l'Académie des sciences. Série 2, Mécanique, Physique, Chimie, Sciences de l'univers, Sciences de la Terre* 307(19), 1981-1986.
- Strang, G. 1988. *Linear Algebra and Its Applications*. Hartcourt Brace Jovanovich College Publishers.
- Tadjou, J. M., Nouayou, R., Kamguia, J., Kande, H. L., Manguelle Dicoum, E. 2009. Gravity analysis of the boundary between the Congo Craton and the Pan-African belt of Cameroon. *Austrian Journal of Earth Sciences* 102(1).
- Tarantola, A., Valette, B. 1982. Generalized nonlinear inverse problems solved using the least squares criterion. *Reviews of Geophysics* 20(2), 219-232.
- Tontini, F. C., Cocchi, L., Carmisciano, C. 2008. Potential-field inversion for a layer with uneven thickness: the Tyrrhenian Sea density model. *Physics of the Earth and Planetary Interiors* 166(1-2), 105-111.
- Tukey, J. W. 1974. Nonlinear (nonsuperposable) methods for smoothing data. *Proceedings of Congress Record EASCOM*, 673-681.
- Ulrych, T. J., Freire, S., Siston, P. 1988. Eigenimage processing of seismic sections. *International Society of Exploration Geophysicists Technical Program Expanded Abstracts*, 1261-1265.
- Vasco, D. W. 1989. Resolution and variance operators of gravity and gravity gradiometry. *Geophysics* 54(7), 889-899.
- Vrabie, V. D., Mars, J. I., Lacoume, J. L. 2004. Modified singular value decomposition by means of independent component analysis. *Signal Processing* 84(3), 645-652.
- Xia, J., Sprowl, D. R. 1992. Inversion of potential-field data by iterative forward modelling in the wavenumber domain. *Geophysics* 57(1), 126-130.
- Zhao, B. B., Chen, Y. Q. 2011. Singular value decomposition (SVD) for extraction of gravity anomaly associated with gold mineralization in Tongshi gold field, Western Shandong Uplifted Block, Eastern China. *Nonlinear Processes in Geophysics* 18(1), 103.

